

RedunCut: Measurement-Driven Sampling and Accuracy Performance Modeling for Low-Cost Live Video Analytics

Gur-Eyal Sela¹, Kumar Krishna Agrawal¹, Bharathan Balaji*², Joseph Gonzalez¹, and Ion Stoica¹

¹UC Berkeley

²Amazon

Abstract

Live video analytics (LVA) runs continuously across massive camera fleets, but inference cost with modern vision models remains high. To address this, dynamic model size selection (DMSS) is an attractive approach: it is content-aware but treats models as black boxes, and could potentially reduce cost by up to $10\times$ without model retraining or modification. Without ground truth labels at runtime, we observe that DMSS methods use two stages per segment: (i) sampling a few models to calculate prediction statistics (e.g., confidences), then (ii) selection of the model size from those statistics. Prior systems fail to generalize to diverse workloads, particularly to mobile videos and lower accuracy targets. We identify that the failure modes stem from inefficient sampling whose cost exceeds its benefit, and inaccurate per-segment accuracy prediction.

In this work, we present RedunCut, a new DMSS system that addresses both: It uses a measurement-driven planner that estimates the cost-benefit tradeoff of sampling, and a lightweight, data-driven performance model to improve accuracy prediction. Across road-vehicle, drone, and surveillance videos and multiple model families and tasks, RedunCut reduces compute cost by 14-62% at fixed accuracy and remains robust to limited historical data and to drift.

1 Introduction

Live video analytics (LVA) performs continuous inference on camera streams to detect events and trigger real-time actions. It now underpins public safety, traffic, retail, industrial, and consumer applications [1–6], with deployments spanning millions of concurrent video streams across edge-cloud infrastructure [6–12]. Since state-of-the-art vision model inference is expensive per frame [7, 13–19] and total cost grows roughly linearly with video volume (number of videos, frame rates, duration) [20], the cost of processing a single 30 fps video stream can exceed \$1,000/month [7]. At scale, the accuracy-cost tradeoff dominates system design.

Beyond growth in scale and cost, LVA applications have broadened along two axes. **First**, sources are increasingly mobile: improvements in cellular and Wi-Fi networks [21–23] enable inference on video feeds from road vehicles and UAVs [24–27], extending existing uses (e.g., license-plate queries for AMBER alerts, on-road hazard detection [28–30]) and enabling new ones (e.g., search-and-rescue, wildfire spotting, crop monitoring [31–33]). **Second**, accuracy targets span a wide range: safety-critical tasks demand high accuracy (e.g., weapon/intruder detection, drone-assisted search-and-rescue [34–36]), whereas cost-sensitive analytics tolerate approximate answers and aggregates (e.g., foot-traffic/occupancy estimation [4], signage/lane-marking defects and pothole detection from dashcams [37]). Consequently, an LVA system must serve both ends, delivering high accuracy as well as inexpensive, approximate analytics when requested.

Goals. Our goal is to create an LVA system that minimizes compute cost while meeting the application’s specified accuracy target. This should be done while serving applications running on a range of video workload types (mobile and stationary) as well as a range of accuracy targets (low to high).

Methods to improve LVA. Existing methods to improve LVA can be classified as (i) *content-agnostic* and (ii) *content-aware*. Content-agnostic methods ignore video content and optimize cost and accuracy via dynamic batching, placement, and accelerator tuning [38–41]. They use the same model size throughout the video (*static model size selection*) and do not adapt resource allocation to the video content, missing cost-reduction opportunities. To fill this gap, recent content-aware works adapt resource allocation across different parts of the video based on content (e.g., dynamic model training [6, 7], early-exit mechanisms [42, 43], and mixture of experts [44, 45]). While these works achieve greater cost reduction, many modify base model weights or architectures and require significant machine-learning expertise to port to new tasks, workloads, and model types.

Opportunity: Dynamic model size selection (DMSS). In contrast, *dynamic model size selection* is a different content-aware method that treats the models as black boxes (no modi-

*Work unrelated to Amazon

fication), and allows the use of off-the-shelf pretrained model zoos, which simplifies development, reduces engineering effort, and speeds deployment while still meeting the application’s accuracy target. In DMSS, the video is divided into segments (e.g., 2 seconds [46]), and a different model size is used to process each video segment. This approach exploits the fact that the accuracy of different model sizes changes across video segments. A smaller, inexpensive model is used on video segments where its accuracy is high, while the larger model is reserved for the rest of the video segments. For example, with an accuracy target of 33.9 MOTA, EDet-D3 (a “small” model with average accuracy of 27.08) still exceeds the target on 31.7% of the video segments, and can be selected in those video segments. Indeed, we find that using DMSS can achieve up to 10× lower cost than static model size selection while preserving the accuracy target (§2).

The use of prediction statistics in DMSS. Selecting the best model size in each video segment requires determining the accuracy of all candidate model sizes on each video segment at runtime. The optimal solution, which runs all models on all frames and compares the predictions to ground truth labels (e.g., human annotations), cannot be used: First, it costs more than a static selection method that runs the largest, most-accurate model alone. Second, the ground truth labels are infeasible or too expensive to access at runtime. Instead, current systems combine two alternatives (Figure 2). First, they evaluate only a few *exemplar frames* (e.g., the first few frames) and extrapolate accuracy to the rest of the segment. Second, they replace using ground-truth labels with properties of model predictions that correlate with the accuracy (e.g., confidence, entropy, disagreement score, sum of objectness scores [6, 7, 47–52]). We collectively refer to these properties as *prediction statistics*. Together, the processing of each video segment at runtime can be broken into two stages: (i) *sampling*: one or more of the model sizes are sampled by running on exemplar frames to get their predictions, and using these predictions to calculate the prediction statistics. (ii) *selection*: These prediction statistics are used to select the model size that optimizes cost and accuracy on the entire video segment. This process is repeated in each video segment to adapt to changing video content.

Challenges when using prediction statistics: sampling and selection (§2).

1. *What is the optimal subset of model sizes to sample on the exemplar frames to calculate prediction statistics?* Sampling too many or too few model sizes may both result in prohibitively high cost. The optimal number of models to sample also widely varies across video segments.
2. *Given only a subset of prediction statistics, which model size to select to run on the entire video segment?* The decision must be made from prediction statistics that may only weakly correlate with the accuracy.

Existing works use manually-crafted rules for both steps: sample all model sizes once then fix a size for the rest of the

video [50, 53]; cascades that sample from small to large with early exits [47–49, 51, 54]; or more elaborate rule sets [46]. These manually-crafted rules are tuned for surveillance workloads and high-accuracy targets. However, in mobile-camera workloads (e.g., road vehicles, drones) and at lower accuracy targets, we see up to 75% higher cost than the static selection baseline. We isolate two factors that drive this gap (§3):

A. Inefficient sampling. Sampling each additional model has two opposing effects: (i) Cost: Sampling increases cost, and (ii) Benefit: Sampling may also reveal a prediction statistic that can be used to select a better model size, e.g., a smaller, less expensive model that preserves accuracy. Existing works do not estimate the *net effect* of sampling and often sample when the cost exceeds the expected benefit, resulting in a net cost increase.

B. Suboptimal selection. The relationship between prediction statistics and accuracy is weak and varies across video segments and workload types. Using thresholds [49, 50, 53] and heuristic rules [46] misses this complexity, resulting in suboptimal model size selection even when sampling is adequate.

Implications. A better approach must (i) estimate the net value of each potential model to sample, and (ii) better capture the relationship between the prediction statistics and the accuracy to improve accuracy prediction, and thereby model size selection.

To implement these design principles and achieve the cost-saving and simplicity advantages of dynamic model size selection across different accuracy targets and workload types, in this paper we propose RedunCut, a new live video analytics system.

Solution. System overview: RedunCut dynamically selects the model size for different segments throughout the video. It is a model-agnostic shim-layer that bolts on top of any prediction-serving system, and has a **control plane** (containing the *sampler* and the *selector*) and a **data plane** that runs the selected model size. The sampler runs a sequential, measurement-driven planner on the exemplar frames to decide which models to sample, producing prediction statistics. The selector uses these prediction statistics and a lightweight, learned accuracy performance model to predict the accuracy, which is used to select the best model size. The data plane runs the selected model size on the entire video segment.

Sampling: measurement-driven planner. RedunCut uses the key insight that prediction statistics of different model sizes correlate with each other (§3). Leveraging this insight, RedunCut uses the prediction statistics of models that were sampled to narrow the range of the possible values of prediction statistics of model sizes that were not sampled yet. This narrower range of values is used by RedunCut’s measurement-driven planner to better estimate the net effect of sampling models that were not sampled yet.

Selection: Accuracy performance model. Prediction statistics are imperfect *proxy metrics* for accuracy, and their rela-

relationship to accuracy varies across workloads and model families (§3.3). We therefore treat accuracy prediction as a *performance modeling* problem: we use a learned, lightweight predictor that maps available prediction statistics to each model’s accuracy, analogous to systems that use purpose-built performance models to predict target metrics (e.g., latency/throughput) from noisy proxy metrics at runtime [55–57]. RedunCut uses a lightweight kNN model that is robust to missing prediction statistics. Its accuracy predictions are used to select the model size in each video segment.

Evaluation. We evaluate RedunCut on instance segmentation and multi-object tracking across six combinations spanning three model families (EfficientDet [14], YOLO [16], DETR [58]), and three video workload types (surveillance, road vehicles, drones). Compared with state-of-the-art baselines [7, 46, 48, 49], RedunCut lowers GPU cost by 14-62% for the same target accuracy. RedunCut remains robust when the historical workload data (*i*) is reduced by 8×, (*ii*) undergoes data drift, or (*iii*) when ground-truth labels are machine-generated. In ablation studies, we find that on average 61% of the cost reduction is achieved by using the new sampling approach, while the rest of the improvement comes from better accuracy prediction during selection. We also find that RedunCut’s accuracy prediction has 3.5 – 10× lower error versus rules used in existing works.

In summary, our paper’s contributions are the following:

1. To our knowledge, this is the first study to investigate dynamic model size selection in mobile video sources. We show that estimating the cost-benefit of sampling and learning the weak and variable relationships of prediction statistics and accuracy is essential to improve performance in such videos.
2. We develop a system (RedunCut) that integrates these insights to generalize to a wide variety of video workload types and accuracy targets.
3. We evaluate this video analytics system and find that it reduces cost by 14-62% over existing methods for the same accuracy target across different video workload types, model architectures, and tasks.

2 Background and Motivation

System goals. The LVA system aims to minimize the cost, i.e., the total computational cost (e.g., GFLOPs) spent on processing the videos, while meeting the application’s accuracy target, i.e., the aggregate accuracy of the predictions on the videos’ frames.

Determining the optimal model size. To achieve optimal DMSS, it is necessary to know both the cost and accuracy in each video segment. For example, Figure 1 (top) shows the accuracies of EfficientDet [14] models of varying sizes in a video. The accuracies are computed over 2-second segments along the video. By knowing the accuracy of different model sizes, the system can determine the best model sizes in each video segment that minimize total cost while meeting the

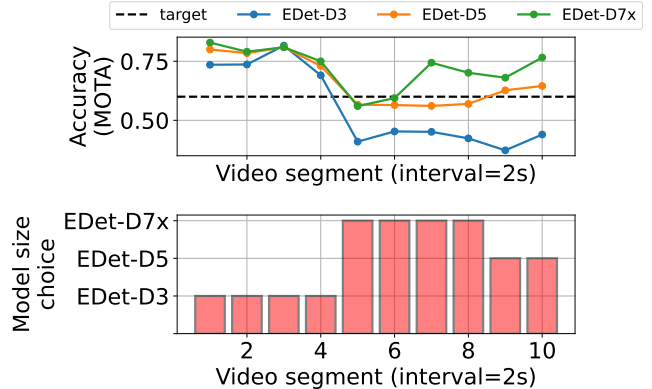


Figure 1: The accuracy of various model sizes in a 20 second video (top), and the resulting model size selection (bottom). Top: The accuracy (y-axis) of different model sizes (color) on 2-second video segments of a road vehicle video (x-axis). Bottom: The resulting model size selection (y-axis) for each video segment (x-axis). The models are taken from the EfficientDet (EDet) [14] family.

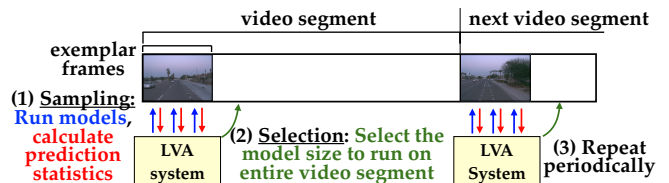


Figure 2: Periodic sampling and selection.

aggregate accuracy target (Fig. 1, bottom). Over many videos, optimal dynamic model size selection (Figure 3 left, blue) can reduce cost by up to 10× when compared to the static selection (“sample once”), which selects and fixes the same model size for the entire video.

Prediction statistics. To overcome the absence of ground-truth labels at runtime, prior works use *prediction statistics* calculated from model predictions [6, 7, 46, 47, 49–52, 59, 60]. These prediction statistics typically require only a few arithmetic operations on model predictions (e.g., summing objectness scores [51, 52, 60]) and are therefore inexpensive to compute. These works use the prediction statistics as indicators for the accuracy in order to select the model size to run on the video segment. This is done in many settings, including perception tasks [49, 51, 61], as well as other modalities [62–65].

Using historical workload data to set sampling/selection parameters. The use of prediction statistics often introduces system parameters (e.g. the confidence score threshold of model cascade [48, 49, 51]) that control how models are sampled and selected [7, 46, 49]. Determining the parameter values analytically is complex. Therefore, existing works [6, 7, 46, 49, 51] rely on historical workload data that is representative of the video content encountered at runtime. This data is used to search for the best set of parameter values that allows the system to optimize the cost and accuracy.

Challenges in sampling. Sampling too many models or none at all is suboptimal. For example, we find (Figure 3, left) that sampling every model in every segment (checkered gray bar, representing a high-sampling version of one DMSS method, Tiered-sampling [46]) drives cost above the static selection (red “sample-once” bar). At the other extreme, never sampling throughout the video results in performance equal to that of the static selection, losing the potential savings of DMSS. The challenge is therefore to strike a balance.

In addition, we find that the optimal number of models to sample varies across video segments and videos, as well as across workload types and accuracy targets (Figure 19, §F).

Challenges in selection. After a subset of the models is sampled, first, their prediction statistics are implicitly or explicitly used to estimate the accuracy, and then the estimated accuracy is used to select the best model size. However, as shown in Figure 6, the prediction statistics often only have a weak correlation (e.g., < 0.4) with the accuracy. It is very uncommon that the correlation is strong (e.g., > 0.8), which would indicate a direct, linear relationship between the prediction statistics and the accuracy. These results suggest that the relationship between the prediction statistics and the accuracy is often weak and potentially noisy. Since the best model size to select is determined from the accuracy, the lack of a strong linear relationship between the prediction statistics and the accuracy makes it challenging to determine the best model size from the prediction statistics.

3 RedunCut’s Solution approach

We first describe the problem with existing works that use manually-crafted rules for sampling and selection (§3.1). Then, we present our ideas to improve sampling (§3.2) and selection (§3.3), which guide the design of RedunCut.

3.1 Problem with existing works

Prior DMSS methods [46, 49, 51, 53] decide which model to run by using manually-crafted rules for *sampling* and *selection*. These rules were developed for static-camera workloads (e.g., surveillance) and for high accuracy targets. As expected, on surveillance videos these methods (e.g., cascade [48, 49, 51, 54], Tiered-sampling [46]) beat the simple baseline that selects and fixes one model size for the rest of the video (*sample-once*); see Figure 3, left. However, when we adapt the same methods to mobile-camera workloads (e.g., road vehicle video) and to lower accuracy targets, the results flip: they cost *more* than the sample-once baseline in low-to-medium accuracy targets (Fig. 3, right).

To understand the cause, we separate the effect of sampling from the effect of selection using two diagnostic variants:

(a) Inefficient sampling. We first remove the cost of sampling from existing works (Tiered-sampling) while keeping the original selection rules (*no-cost sampling*, Fig. 3 right). The remaining gap to “sample-once” reflects the cost savings

achieved by DMSS alone. On road vehicle videos, this gap is small (e.g., $\sim 20\%$ cost reduction at 28 MOTA, Fig. 3 right). This gap is *less* than the cost of sampling that was removed. Together, the models that these methods sample often do not “pay for themselves,” so total cost increases.

(b) Suboptimal selection. Next, we also replace the original selection rules with oracle selection, which has access to the true accuracy that each model would achieve on the segment (*no-cost sampling + oracle accuracy*, Fig. 3, right). This hypothetical variant cuts cost by as much as 50% relative to no-cost sampling, indicating that the accuracy prediction used by current selection rules to select a model size has too much error, resulting in suboptimal model size selection.

3.2 Improving sampling

Analysis of sampling. Sampling a model M has two opposing effects:

1. The **cost** of running M on the exemplar frames (to get its predictions and calculate the prediction statistic).
2. The potential **benefit** from changing to a better model size selection given the calculated value of the prediction statistic of model M (e.g. reduction in cost of the selected model for the same accuracy).

For clarity, we will refer to these as component (i) and component (ii), respectively.

Sampling should happen when the net effect is positive, i.e. component (ii) $>$ component (i). Existing works [46, 48, 49, 51, 53] do not explicitly estimate these components. Instead, they use rules that incorporate fixed assumptions about their relative effect. We propose to explicitly estimate and compare these components at runtime.

Estimating the benefit (component (ii)). Component (i) is known upfront, before sampling, as a fixed cost of model inference. In contrast, component (ii) is the benefit we might get *after* sampling, when model M ’s prediction statistic causes the system to switch to more optimal model size. Since the prediction statistic is only revealed after sampling, we cannot know the exact benefit at decision time. To overcome this, we *estimate* the benefit in advance from historical workload data.

Using historical workload data. Although model M ’s prediction statistic is unknown before sampling, its *distribution* can be estimated from historical workload data. Using empirical frequencies of past video segments (Figure 5, blue), we assign probabilities to each possible value and compute the *expected value* of the benefit (component (ii)). This expected value is compared against the known sampling cost (component (i)) to decide whether to sample model M .

Example 1. Consider a system with three model sizes (Small, Medium, and Large), with selection costs of 30, 55, and 100, respectively (Figure 4). The objective (as used in prior work [46, 49]) is to select the least expensive model size whose accuracy has at least 90% chance of being above the

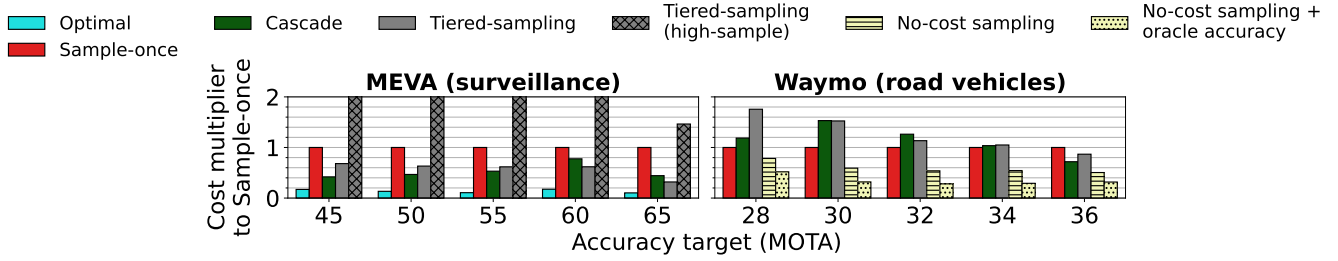


Figure 3: The cost of various model size selection methods in different video workload types and accuracy targets. The cost (y-axis) of various model size selection methods (color, bar pattern), normalized to the cost of the sample-once method (red) in surveillance (left panel) and road vehicle camera (right panel) video workloads across several accuracy targets (x-axis). Bars with patterns (e.g. Tiered-sampling (high-sample)), represent hypothetical solutions.

accuracy target. We consider two possible sampling decisions and estimate component (i) and (ii) to decide which is better:

(a) No sampling (baseline). Historical workload data indicates (Fig. 4, top center) that the Small, Medium, and Large model’s accuracies exceed the target in 20%, 70%, and 100% of the video segments. Without sampling, Large must be selected (cost=100).

(b) Sampling the Large model. We sample Large (cost=10), and calculate its prediction statistic, the sum of objectness score across all objects in the frame [51, 52]. A high score indicates that the video segment’s scene is busy, and thus more challenging: More chance for small objects, occlusions, or unusual angles that are harder to detect. If the Large model is sampled, its prediction statistic has three possible values: A, B, and C (representing a low, medium, and high objectness score). Historical data show (Figure 4, bottom):

1. If the prediction statistic is A: All models meet target → select Small (cost=30)
2. If B: Medium and Large meet target → select Medium (cost=55)
3. If C: Only Large meets target → select Large (cost=100)

The *expected value* of the selection cost after sampling = $0.2 \times 30 + 0.5 \times 55 + 0.3 \times 100 = 63.5$. The benefit from improving selection (component (ii)) = $100 - 63.5 = 36.5$, which exceeds the sampling cost (component (i))=10. Therefore, sampling the Large model is preferred over no sampling.

Using correlations between prediction statistics. Before sampling, we only have a broad range for a model’s prediction statistic based on all past segments (Figure 5, blue), making our benefit estimate (component (ii)) imprecise. To narrow down this range of potential values, we observe that the prediction statistics of different model sizes show a moderate to strong correlation (0.6-0.9) across workload types, prediction statistic types, and model families (§H). This means that prediction statistic values tend to move together, so the value of one model’s prediction statistic helps narrow down the likely values of other prediction statistics of models that weren’t sampled yet, improving component (ii)’s estimate.

This is shown in Fig. 5: The blue histogram shows model

Model size	Sampling cost	Selection cost	Model size	% of video segments where accuracy > target	Objective: To select the least expensive model that has at least 90% chance of accuracy > target
Small	5	30	Small	20	
Medium	7	55	Medium	70	
Large	10	100	Large	100	

Large model's Prediction statistic values	% of video segments (out of all)	% of video segments (in which med pred. stat = L)	Predicted accuracy	Selected model size	Selection cost
A	20	80	Small, medium, large > target	Small	30
B	50	18	Medium, large > target	Medium	55
C	30	2	Large > target	Large	100

Figure 4: Example for the use of historical workload data to estimate components (i) and (ii). Top left: The costs of sampling and selection. Top center: Predicted accuracy when no models are sampled. Bottom: Varying outcomes of sampling Large, based on the prediction statistic value in the video segment. See text for details.

EDet-D7X’s prediction statistic distribution across all video segments. When the historical data is filtered only to segments where EDet-D5’s statistic=3, the likely range of EDet-D7X’s prediction statistic narrows markedly. Multiple sampled models compound this effect: Filtering by both EDet-D5=3 and EDet-D7=4 (green) narrows the likely values further.

Example 2: A narrower value range flips the sampling decision. Suppose we already sampled the Medium model and its prediction statistic is *L*. With this observation, the tentative selection is the Medium (meets >90% objective) with cost 55. Now, consider three options:

1. **No further sampling (baseline).** Keep Medium selection, cost=55
2. **Sample Large using overall frequencies (ignoring L).** From historical data (Fig. 4, bottom), the Large models’ prediction statistic values A, B, C occur in 20%, 50%, and 30% of the video segments. Following the same analysis in the previous example: The sampling cost (component (i)) = 10, the expected selection cost = 63.5, so the change in cost from updated selection (Component (ii)) = $55 - 63.5 = -8.5$. Component (ii) < component (i) → Don’t sample.
3. **Sample the Large model using the filtered frequencies (taking L into account).** Historical data filtered by L (Fig. 4 (bottom)) shows that A, B, C occur in 80%, 18%, and 2% of the video segments (the frequencies become

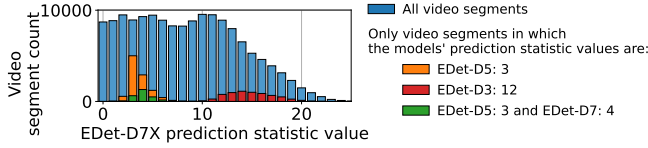


Figure 5: Using the historical workload data (filtered and unfiltered) to get the range of likely values of prediction statistics. The histogram of the prediction statistic (sum of objectness score [51,52]) of model EDet-D7X [14] in different video segments of the historical workload data (road vehicles videos [66]). The histogram is shown unfiltered for all video segments (blue), and filtered: only for segments where EDet-D5=3 (orange), only for segments where EDet-D3=12 (red), and only for segments where EDet-D5=3 and also EDet-D7=4 (green).

concentrated on A (80%). The sampling cost (component (i)) is 10, but now the expected value of the selection cost = $0.8 \times 30 + 0.18 \times 55 + 0.02 \times 100 = 35.9$, so component (ii) = $55 - 35.9 = 19.1$. Since component (ii) > component (i) \rightarrow Sample the Large model (decision flipped!).

Takeaway. Using historical workload data (Ex. 1) and filtering it using the prediction statistics of previously-sampled models (Ex. 2) yields explicit (and more precise) estimates of component (ii), which can be used to decide which model to sample and which to avoid.

3.3 Improving selection

Varying and weak correlation between prediction statistics and accuracy. Selection depends on predicting each model’s accuracy from prediction statistics. These statistics (e.g. prediction confidence score) are imperfect *proxy metrics* for accuracy. Figure 6 shows that the Pearson correlation between each model size’s prediction statistic (x-axis) and the accuracy of other models (y-axis) ranges from nearly 0 to ≈ 0.8 , and varies substantially with workload type, prediction statistic, and model family (similar trends using Spearman correlation are shown in §E).¹ This variation implies that simple hand-crafted rules (e.g., single-variable thresholds or formulas [46–49,51]) will not predict the accuracy well across all settings, motivating a more robust approach.

Adopting a performance modeling perspective. We view predicting accuracy from prediction statistics as a *performance modeling* problem. In systems scheduling, performance models are widely used when the mapping from task configuration and proxy metrics (e.g., % CPU utilization) to the end-to-end metric (e.g., latency) is complex and platform-dependent [55–57,70–74]. Our setting is analogous: the mapping from prediction statistics to accuracy depends on complex interactions between the model and the input distribution and can vary across models and workload types.

¹More broadly, prior work shows the relationship between common prediction statistics and accuracy can be non-linear and dataset- and model-dependent [67–69].

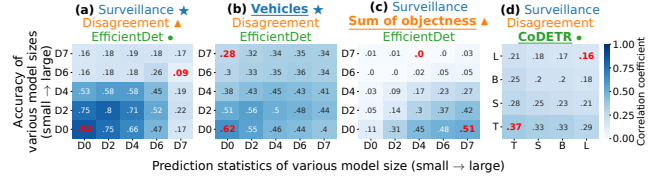


Figure 6: The varied correlation between prediction statistics and accuracy. The correlation (Pearson) between the prediction statistics (x-axis) and the accuracy (y-axis) across different model sizes. Heading: Blue: Workload type. Orange: Prediction statistic type. Green: Model type. The correlation varies depending on the workload type ((a) vs (b)), prediction statistic ((a) vs (c)), and model type ((a) vs (d)). The maximum and minimum values in each heatmap are emphasized (bold/red).

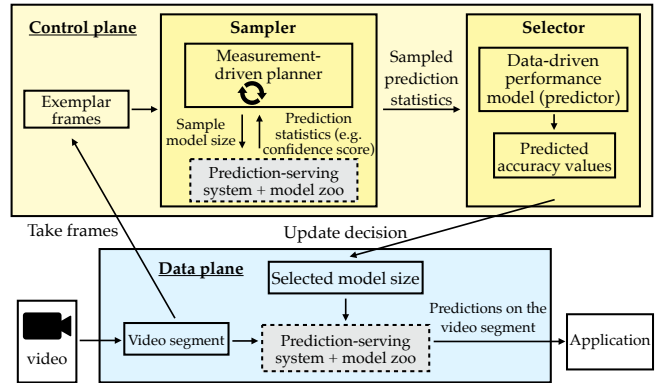


Figure 7: RedunCut’s architecture and workflow.

A data-driven performance model for accuracy. We therefore use a learned performance model [55, 56, 72] that leverages historical workload data to predict the accuracy of each model size from prediction statistics. Compared with manually-crafted rules, a learned model can combine multiple weak proxy metrics and remain robust in the presence of noise [57, 74]. In §5.5, we show this data-driven approach improves accuracy prediction substantially ($3.5\times-10\times$ lower error versus manually-crafted baselines), which in turn improves model selection.

These key insights (explicit cost-benefit analysis for sampling and using a data-driven accuracy performance model for selection) guide RedunCut’s design.

4 RedunCut Design

RedunCut is a dynamic model size selection system for live video analytics. Its goals are (i) simplicity: no changes to the base-models or additional training, and (ii) cost reduction by adapting model size to video content. RedunCut works with any prediction-serving system and model zoo (Figure 7). It consists of a control plane for sampling and selection and a data plane that executes the selected model size. The control and data planes are separated to keep selection off the critical path (§4.4) and give the data plane priority when selection and execution call the same prediction-serving system.

RedunCut’s workflow (Figure 7). For each new video segment, exemplar frames are sent to the control plane. Inside the sampler (§4.2), a measurement-driven planner uses historical workload data to guide an iterative sampling process that efficiently determines which model to sample or avoid. The prediction statistics of the models sampled are passed to the selector (§4.3), which uses a data-driven performance model to predict each model’s accuracy. RedunCut then calculates the cost-accuracy objective (§4.1) for each model, selects the best model size, and sends the selection back to the data plane to run on the video segment.

4.1 Objective

The application’s cost and accuracy goals are calculated in aggregate over all videos at the end of execution. In contrast, at runtime, LVA processing only has access to past videos. Therefore, different works [46, 49, 50] use a surrogate objective to guide sampling and selection in each video segment.

RedunCut uses a scalarized objective that linearly combines normalized accuracy and cost in a single expression, using a tunable trade-off parameter $\alpha \in [0, 1]$:

$$\text{cost_acc_obj} = \alpha \times \text{cost} + (1 - \alpha) \times (1 - \text{acc}) \quad (1)$$

This objective is simple to calculate and is used extensively in utility and objective functions in prior work [50, 75, 76].

4.2 Efficient Sampling

§3 shows how historical workload data can be used to estimate component (ii), and that as more prediction statistics are known, the estimates and the sampling decisions improve.

Sequential operation. To maximally exploit these ideas, RedunCut avoids sampling models in parallel, which precludes using one model’s prediction statistic to improve sampling for other models. Instead, we design a measurement-driven planner that samples sequentially, one model at a time. This allows using the observed prediction statistics of all previously sampled models in order to get increasingly precise estimates of component (ii) for the next model to sample.

This sequential sampling design abides by anytime semantics: As more iterations are run, more cost is expected to be saved since each additional iteration is designed to improve the objective through careful estimation of component (ii).

Probability estimation from historical workload data. Component (ii) is estimated using the expected value of the prediction statistic of the model m considered for sampling. This requires estimating $p_m(s|\mathcal{O})$, the probability that prediction statistic value s will be calculated after sampling model m on the video segment, given prediction statistics set \mathcal{O} observed from previously sampled models. Since the sampling process may repeatedly query $p_m(s|\mathcal{O})$ to calculate the expected value, its estimation must be computationally inexpensive and fast. Therefore, we use empirical probability

estimates for $p_m(s|\mathcal{O})$ based on observed frequencies in the historical data [77–79].

Let $\mathcal{O} = \{(m_i, s_i)\}_{i=1}^k$, where prediction statistic s_i was observed for model m_i in the current video segment. Define $N(\mathcal{O})$ to be the number of video segments in the historical data in which these prediction statistics were also observed:

$$\hat{p}_m(s|\mathcal{O}) = \frac{N(\mathcal{O} \cup \{(m, s)\})}{N(\mathcal{O})} \quad (2)$$

Continuous prediction statistics (e.g. confidence score [48], sum of objectness score [51]) are discretized via binning. The number of bins is tuned for each workload type based on the historical data. We found that using 10-20 bins for each prediction statistic is a good default across workload types.

Sampling planner overview. The planner operates iteratively: (1) Estimate component (ii) and the net benefit (component (ii) - component (i)) for each unsampled model, (2) Sample the model with the highest net benefit, stopping when no models have positive net benefit. To estimate component (ii), the planner calls the selector and the accuracy prediction model (§4.3) for each potential prediction statistic value.

Estimating component (ii). We define $J(\mathcal{O})$ as the objective when selecting based on the prediction statistics in \mathcal{O} :

$$J(\mathcal{O}) = \text{Objective}(c(\text{Select}(\mathcal{O})), \hat{a}(\text{Select}(\mathcal{O}), \mathcal{O})) \quad (3)$$

$\text{Select}(\mathcal{O})$ is the model selected by the system based on prediction statistics \mathcal{O} (§4.3), $c(\cdot)$ is the model’s selection cost, \hat{a} is the predicted accuracy of the model (§4.3), and Objective is the objective function (Eq. (1)).

Component (ii) is then estimated as:

$$\begin{aligned} \text{Component ii}(m, \mathcal{O}) &= \\ &\mathbb{E}[J(\text{pred. stats before sampling})] \\ &- J(\text{pred. stats after sampling}) = \\ &J(\mathcal{O}) - \sum_{s \in \mathcal{S}_m} \hat{p}_m(s|\mathcal{O}) \times J(\mathcal{O} \cup \{(m, s)\}) \end{aligned} \quad (4)$$

Where \mathcal{S}_m is the potential values that model m ’s prediction statistic can take. Using Eq. (4), the full sampling routine for a new video segment is shown in Algorithm 1.

Data drift and outlier detection. At runtime, sampling yields various combinations of values of different prediction statistics (\mathcal{O}). To ensure we only trust probability estimates $\hat{p}_m(s|\mathcal{O})$ that are sufficiently supported by data, RedunCut requires at least T_{min} matching video segments (by default $T_{min} = 10$) in the historical data. If the matched count falls below T_{min} , the video segment’s prediction statistic combination \mathcal{O} is treated as underrepresented in the data. In this case, RedunCut halts sampling, removes the last prediction statistic from \mathcal{O} whose inclusion caused the count drop, and passes the remaining prediction statistics to the selector. This approach allows RedunCut to avoid inflating cost by running long sampling sequences on new video data not sufficiently represented in the historical data. In the extreme, if an outlier is detected

Algorithm 1: Measurement-driven sampling planner

Input: Candidate models \mathcal{M} **Output:** Prediction statistics \mathcal{O}

```
1  $\mathcal{O} \leftarrow \emptyset$  // Observed (model, stat) pairs
2 while true do
3   foreach unsampled  $m \in \mathcal{M}$  do
4      $G[m] \leftarrow \text{Comp. } ii(m, \mathcal{O}) - \text{SAMPLECOST}(m)$ 
      // Eq. (4)
5     if  $\max_m G[m] \leq 0$  then
6       return  $\mathcal{O}$ 
7      $m^* \leftarrow \arg \max_m G[m]$ ;  $s \leftarrow \text{SAMPLE}(m^*)$ ;
8      $\mathcal{O} \leftarrow \mathcal{O} \cup \{(m^*, s)\}$ 
```

Algorithm 2: Selector

Input: prediction statistics \mathcal{O} , candidate models \mathcal{M} **Output:** Selected model m^*

```
1 foreach  $m \in \mathcal{M}$  do
2    $\hat{a}[m] \leftarrow \text{ACCURACYPREDICT}(m, \mathcal{O})$  // §4.3
3    $obj[m] \leftarrow \text{Objective}(c(m), \hat{a}[m])$  // §4.1
4  $m^* \leftarrow \arg \min_{m \in \mathcal{M}} obj[m]$ ; return  $m^*$ 
```

after sampling the first model, RedunCut immediately falls back on the default model size for $\mathcal{O} = \emptyset$. This mechanism gracefully handles severe data drift. We extensively evaluate robustness to drift in §5.4.

4.3 Data-driven accuracy prediction

Selector overview. As shown in Algorithm 2, the selector predicts the accuracy of each candidate model size and chooses the one that minimizes the cost-accuracy objective.

Accuracy performance model. RedunCut uses a learned performance model to capture complex interactions between prediction statistics and accuracy. The performance model must: (i) tolerate changing input features (varying \mathcal{O} per segment), (ii) be computationally fast for repeated invocations.

For our design, we use a k-nearest neighbors (kNN) model for accuracy prediction [80, 81]. kNN can naturally handle missing features [81], achieves sub-ms inference on a single CPU core, and requires no training beyond storing historical data. When using kNN for accuracy prediction, the same neighbors (computed from the prediction statistics \mathcal{O}) predict accuracy for all \mathcal{M} models, via model-specific voting, which reduces the number of operations done by the model. When no model has been sampled ($\mathcal{O} = \emptyset$), the predictor returns each model’s average accuracy in the historical data, which results in selecting the best model on average. We tune k and the distance metric on historical data.

Caching. To further reduce the accuracy prediction overhead, RedunCut caches the accuracy predictions for com-

monly repeated combinations of prediction statistics (e.g. the empty set $\mathcal{O} = \emptyset$, when no models have been sampled yet).

4.4 Managing latency

Many video analytics applications impose deadlines of 2-15 sec [50, 82]. Sequential sampling may overrun the deadline because of transient delays in the prediction-serving system (e.g., from cloud contention). To ensure that the best model size selection available is submitted on time for execution, we decouple the control plane (sampling/selection) from the data plane (execution), giving the data plane higher priority.

Workflow. On arrival at time t_{arr} , each video segment is assigned a default model size (the selector’s choice when $\mathcal{O} = \emptyset$) and a control-plane commit timestamp t_{commit} . At each planner iteration (Algorithm 1), the control plane passes the current prediction statistics \mathcal{O} to the selector, obtains a tentative choice m_{curr} , and asynchronously updates $\langle m_{\text{curr}}, t_{\text{commit}} \rangle$. The commit time is:

$$t_{\text{commit}} = t_{\text{arr}} + T_{\text{deadline}} - \hat{q} - \hat{t}_{\text{exec}}(m_{\text{curr}})$$

where \hat{q} is the estimated queuing delay and $\hat{t}_{\text{exec}}(m_{\text{curr}})$ is estimated execution time (from past latency profiles). At t_{commit} , the data plane executes the latest m_{curr} . \hat{q} is estimated via a direct measurement. We leave exploring richer queue wait time prediction for future work.

5 Evaluation

We evaluate RedunCut on road vehicle, drone, and surveillance camera videos in two perception tasks and three model architecture families, making the following findings:

1. RedunCut reduces compute cost by 14-62% over Tiered-sampling [46] and 11-60% over a gating network [7] while maintaining the same accuracy in road vehicle videos.
2. The majority (62% on average) of RedunCut’s performance improvement comes from the sampler.
3. RedunCut remains robust to data drift that results in a mismatch between the historical data and the videos at runtime.
4. Additional sampling iterations monotonically improve performance and contribute to 5%-40% of RedunCut’s overall improvement.

5.1 Experimental setup and methodology

Implementation. RedunCut is implemented using Ray [83], and uses Ray Serve [84] as the prediction serving system. We use separate actor pools for the control and data planes, which communicate asynchronously (§4.4). During runtime, we use nodes with 2 Titan RTX GPUs.

Datasets. We evaluate RedunCut on road vehicle, drone, and surveillance camera datasets, covering a range of camera movement speeds, weather conditions, and times of day.

- **Road Vehicles:** We use the front-facing camera footage in the Waymo [66] dataset. This dataset is composed of 798 training and 202 validation videos, all of length 20 seconds.
- **Drone:** We use the VisDrone [85] dataset, in which videos shorter than 20 seconds are discarded for uniformity (leaving an average video length of 37 seconds). The dataset is composed of 35 training videos and 14 test videos.
- **Stationary camera surveillance:** We use the MEVA [86] dataset of indoor and outdoor wall-mounted security camera footage. The dataset has 28 training and 8 test videos, with video lengths range from 30 seconds to 5 minutes.

Models. To evaluate and compare DMSS methods, we use a range of multi-object tracking and instance segmentation model sizes. The trackers are built using EfficientDet [14], YOLOX [16], or DETR [58] models for detection followed by SORT [87] for tracking. These models span over two orders of magnitude of cost (1.08–410 GFLOP), and range in accuracy from 25.8 to 55.1 mAP. To stay consistent with the methodology of prior works [46, 49, 50], we use model sizes whose cost and accuracy are Pareto optimal. The models are run using TensorFlow [88], and are pretrained on the COCO dataset [89, 90].

Metrics. We evaluate model size selection in multi-object tracking and instance segmentation, both key tasks in video analytics [50, 51]. **Accuracy** is calculated for each task using standard metrics: the MOTA tracking score [91] and the segmentation Average Precision [89], respectively. **Compute cost** is measured using floating-point operations (FLOPs) based on reported values [14, 16]. The final accuracy of a model size selection method is determined as follows: (i) model sizes are selected in the videos (ii) the selected models make predictions on the videos (iii) the method’s accuracy is the aggregate accuracy of these predictions on the videos. The total cost is the average FLOPs/frame performed by the selected models.

Trace-driven simulator. We also built a simulator to test RedunCut under a wide range of configurations, resource constraints, and longer execution times. The simulator takes as input the cached model predictions on the video frames, as well as the inference cost logs. This exhaustive approach allows us to mimic our implementation’s execution with high-fidelity under different constraints.

Comparing methods. Model size selection methods are compared by measuring the minimal compute cost that each method requires in order to meet the same accuracy target.

Setting control parameters. As discussed in §2, several methods [7, 46–48] introduce multiple parameters that control sampling and selection. We run standard random search with the historical workload data to find the optimal parameter value combinations for each method at each accuracy target.

Setup details. Following the prevailing evaluation methodology used in existing works [7, 46, 49, 92], we use generated labels for the MEVA (surveillance) dataset (which lacks

human-annotated labels) via large model prediction. To get high-fidelity predictions, we combine the state-of-the-art detection model DETA [93] and tracking module Unicorn [94].

5.2 End-to-end results

First, we evaluate and compare RedunCut against the following dynamic model size selection methods:

1. **Tiered-sampling:** This is a sampling method used by Chameleon [46] in which expensive sampling is performed infrequently while inexpensive sampling is done more frequently (details on control parameters in §A). To keep evaluation fair, the following complementary methods are not included in the solution: (i) The hill-climbing method is not used because optimization takes place over a single dimension (model size). (ii) Further, our evaluation uses camera feeds that do not share the same space and time dimensions, so the spatial locality approach does not apply.
2. **Gating network:** We adapt the “expert” model selection mechanism in RECL [7] to model size selection. In this approach, a lightweight gating neural network is trained to select the top-k model sizes on a video frame. Afterwards, runtime profiling is used to filter down to the top-1 model size. We adapt RECL’s labeling schema by setting the labels to be the model size choice that best optimizes the cost-accuracy objective. The gating network is then trained in separate trials using labels produced with different threshold values to modulate between cost and accuracy. We use the same routing network architecture as RECL (a ResNet18 [95]). This model size has negligible compute cost.
3. **Cascade:** The model cascade samples models from small to large [47–49]. The model cascade is assembled using the smallest and the largest models used in each dataset (§5.1), following existing works. As far as we know, there are no adaptations of a model cascade to multi-object tracking. Therefore, we develop a straightforward confidence-score based early-exit rule described in §C.
4. **Sample-once** [50, 53]: Static selection in which the optimal model size is determined once at the beginning of the video and fixed for the rest of it. To keep evaluation consistent, the model is determined using the same selection method used by Tiered-sampling [46].

The end-to-end evaluation on surveillance, road vehicle, and drone videos is shown in Figure 8. The figure illustrates the cost of various methods across different accuracy targets. A line is plotted across the cost-accuracy tradeoff points of each method to distinctly visualize them. The results show that RedunCut achieves higher accuracy at a lower cost than the rest of the methods, across a wide accuracy spectrum and across the video workload types. In contrast, the other methods tend to vary in their cost-efficiency compared to one another. Existing works sample and select models using rules that result in inefficient sampling and suboptimal se-

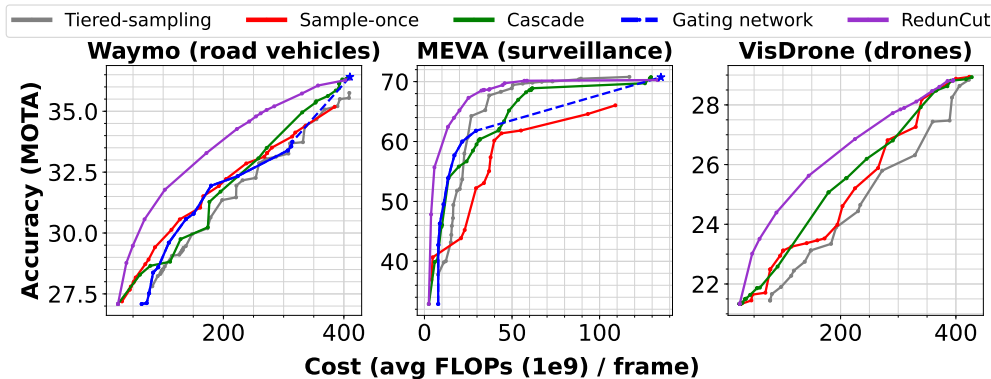


Figure 8: End-to-end cost-accuracy Pareto frontier of RedunCut and other methods evaluated in road vehicle (a), Surveillance (b), and drone (c) videos. The Pareto frontier of each method represents the lowest compute cost (x-axis) that each method requires to reach a certain accuracy (y-axis). §5.1 describes the generation of the Pareto frontier curve. The dashed, blue line is described in §5.2.

lection. Instead, RedunCut achieves significant cost savings by explicitly calculating the net effect of sampling and using data-driven accuracy prediction.

To more clearly compare RedunCut with existing methods, we directly measure the compute cost that each method requires in order to meet a range of accuracy targets. To simplify comparison, the compute cost of every method is normalized by dividing it by the compute cost of the sample-once baseline. Results are shown on the Waymo (road vehicle) dataset in Figure 9. We make the following observations:

Comparison to RedunCut. The performance difference between RedunCut and other methods varies depending on the accuracy target. In road vehicle videos, RedunCut saves 19-62% over the Tiered-sampling method [46] and 11-60% in compute cost over the gating network [7]. Likewise, in stationary camera surveillance videos, RedunCut saves 42-76% over Tiered-sampling and 38-61% over the gating network (§D). Similar improvements are achieved in drone videos (18-67% over Tiered-sampling, see §D).

Gating network limitation. Due to a limitation in the adaptation to model size selection, the gating network’s cost and accuracy do not extend to the top-right of the tradeoff space. This is related to the large fraction of scenarios in which smaller models have equal to or better accuracy than the large model [96] (see §B). To overcome this, we simulate an ideal adaptation of the gating network in which the largest model size is always selected. This gives the highest possible point (dashed blue segment and asterisk in Fig. 8 and translucent blue bars in Fig. 9).

5.3 Generalization

Across model families. Next, we evaluate RedunCut using different model architecture families: The YOLOX [16] (Figure 10 (a)) and the CoDETR model families [58] (Figure 10 (b)). The cost reduction range over Tiered-sampling is 16%-84% for the same accuracy target. The high cost of the cascade baseline in the YOLOX family may be attributed to the wider accuracy gap in the YOLOX models used in the cascade (25.8 and 49.7 mAP) than in the EfficientDet models used in the

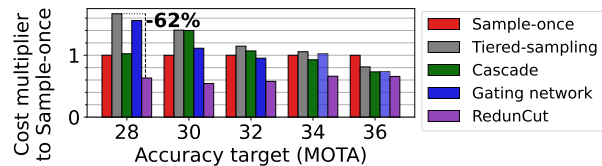


Figure 9: Cost comparison between RedunCut and other methods in road vehicle videos. Each method (color) is evaluated on a range of accuracy targets (x-axis). Each method’s compute cost is normalized by the compute cost of the sample-once method (y-axis). The translucent blue bars are described in §5.2.

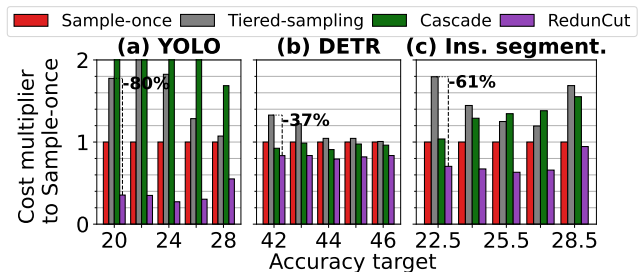


Figure 10: RedunCut’s performance across model families (a [16], b [58]) and tasks (c, instance segmentation). The normalized compute cost (y-axis) of several model size selection methods (bar color) is shown across different accuracy targets (x-axis).

cascade (47.2 vs 55.1 mAP). Thus, when the accuracy gap in the cascade is higher, the larger model selection based on the small model’s confidence score is less optimal, resulting in higher cost.

Across tasks. We evaluate RedunCut in a different task, instance segmentation, using the YOLOX-seg model family [16] and the KITTI-STEP [97] road vehicle dataset. The results (Figure 10 (c)) show that RedunCut improves across all accuracy targets, with a cost reduction range of 44-61%.

5.4 Robustness benchmarks

To further understand RedunCut’s advantages and limits, we conduct evaluation in resource-constrained settings.

Less historical workload data. RedunCut uses the historical workload data for both sampling and selection (§4). Redun-

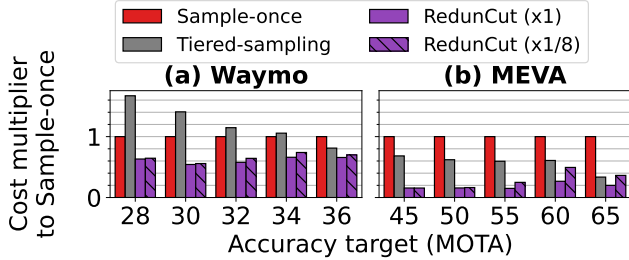


Figure 11: RedunCut’s robustness in settings with less historical workload data. The normalized compute cost (y-axis) of several model size selection policies (bar color) across different accuracy targets (x-axis) in road vehicles (a) and surveillance (b) videos. Historical video data length is reduced from 4.4 hours ($\times 1$) to 0.5 hours ($\times 1/8$) in Waymo and 2.3 hours ($\times 1$) to 0.3 hours ($\times 1/8$) in MEVA.

Cut is designed for video analytics at scale, in which large amounts of historical data are expected to be available. However, to understand RedunCut’s limits, we investigate its performance when historical workload data is scarce. To this end, we reduce the amount of data available to RedunCut by $\times 8$ (Figure 11). The results show that RedunCut’s performance is largely preserved in both Waymo and MEVA datasets (30 minutes and 18 minutes, respectively).

Robustness to drift between historical workload data and runtime videos (location, camera setup, workload type).

Data drift [6, 7, 98] or operational mistakes can make runtime videos differ from RedunCut’s historical data. We evaluate RedunCut by deliberately mismatching historical data and runtime videos along three axes: geography (e.g., San Francisco/Phoenix vs. New York), camera configuration (sensor, resolution, frame rate, mount angle), and workload type (road vehicles vs. static surveillance). In Waymo runtime videos (Figure 12a), when we evaluate location and camera setup mismatches (BDD100k HD, a different road-vehicle workload), cost remains within 5–10% of using matched Waymo historical data. Mismatch in the workload type is tougher: Using MEVA (surveillance) historical data for Waymo runtime further increases cost, while the reverse (Waymo historical data and MEVA runtime) has a smaller effect (Fig. 12a–b). Together, RedunCut reduces cost over existing methods under mixed conditions, and can leverage other video sources when matching videos are unavailable.

Historical workload data without human labeling. Like other methods (§2), RedunCut requires labels in the historical workload data. Obtaining high-quality human labels is costly and time-consuming. A common alternative is to automatically generate labels using a high-accuracy model, an approach adopted by several recent works [6, 7, 46, 50]. Here, in Figure 13, we evaluate RedunCut with historical workload data whose labels were automatically generated. The data’s labels are generated using the largest model available for selection at runtime. Results show that across Waymo (Fig. 13

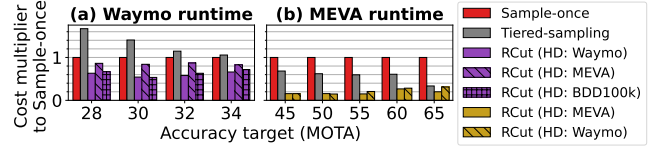


Figure 12: RedunCut’s (RCut) robustness to data drift between historical data (HD) and runtime videos (location, camera setup, workload type). Various combinations of RedunCut’s HD source were mixed and matched with various runtime video workloads: (a) road vehicle and (b) surveillance. The normalized compute cost (y-axis) is shown across different accuracy targets (x-axis). See §5.4.

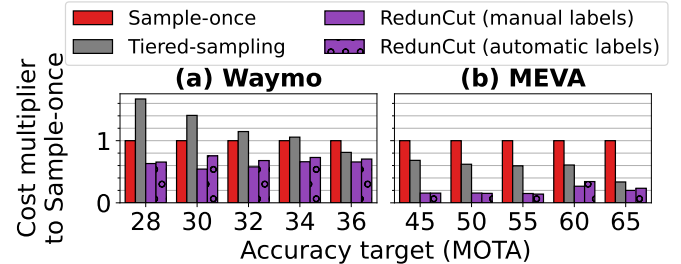


Figure 13: RedunCut’s robustness when the historical workload data is automatically labeled. The normalized compute cost (y-axis) of several model size selection methods (bar color) across different accuracy targets (x-axis) in road vehicle (a) and surveillance (b) videos. Label schema: (i) Manual human labeling (clear, purple) and (ii) Automatic labeling by model (purple with circles).

(a) and MEVA (Fig. 13 (b)), performance remains largely unchanged when automated labels are used. This result broadens the potential use of RedunCut to settings in which human annotation is absent or expensive.

5.5 Analysis of RedunCut’s performance

The contribution of additional iterations in the planner.

In each iteration, RedunCut’s planner only samples model sizes that it estimated to have a positive net effect on cost and accuracy. To quantify the value of additional iterations, we ablate the maximum number of iterations that the planner can do $\{0, 1, 2, 5\}$. The 5-iteration configuration is the full RedunCut solution. With 0 iterations, no sampling is performed: RedunCut simply selects the *best-on-average* model by computing each model’s average accuracy on the historical workload data and using that value as the predicted accuracy when selecting a model size (§4.3).

Figure 14 shows that the benefit of additional iterations increases in higher accuracy targets (x-axis). At low targets (28-30 MOTA) sampling only adds $\sim 5\%$ of RedunCut’s total cost savings, while $\geq 90\%$ of the savings come from the best-on-average model alone. At the highest target (36) sampling accounts for $\sim 40\%$ of the total savings, with the remaining $\sim 60\%$ still coming from selecting the best-on-average model.

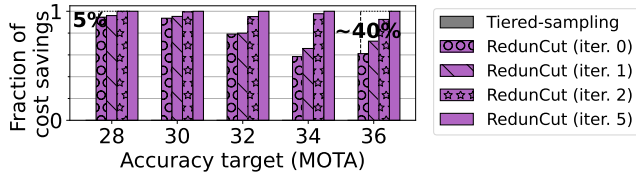


Figure 14: The effect of sampling iterations on RedunCut’s performance. The fraction of RedunCut’s cost savings over Tiered-sampling [46] (y-axis) after a different number of sampling iterations (bar pattern) across accuracy targets (x-axis) in road vehicle videos. Higher y-axis values indicate better performance.

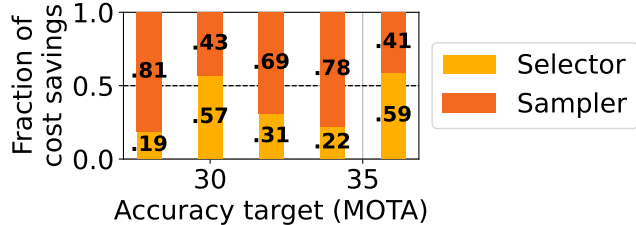


Figure 15: The contribution of the sampler and selector to RedunCut’s performance. RedunCut’s cost improvement over Tiered-sampling [46] (y-axis) contributed by each component (color) across different accuracy targets (x-axis) in Waymo (road vehicle) videos.

Takeaway. In low accuracy targets, a single model size selection using the average accuracy suffices and additional sampling is largely redundant. As the accuracy target increases, additional sampling iterations can help in improving selection between small and large models.

Ablation of sampler vs selector. RedunCut replaces the manually crafted rules in prior work by using two new mechanisms: (i) efficient, measurement-driven sampling by the planner (Secs. 3.2 and 4.2) and (ii) selection via data-driven accuracy prediction by RedunCut’s selector (Secs. 3.3 and 4.3). We quantify each mechanism’s contribution by swapping our sampler with Tiered-sampling [46] while retaining RedunCut’s selector. In Figure 15, both sampling and selection are crucial to RedunCut’s improvement over prior methods; the sampler accounts for 41–81% of RedunCut’s total cost savings. The opposite ablation (RedunCut’s sampler and Tiered-sampling’s selection), shows a similar attribution to performance by the selector (§I), suggesting a degree of overlap in effect.

Error in accuracy prediction. We evaluate RedunCut’s learned performance model (kNN) for predicting accuracy from prediction statistics, and compare it to rules used in prior works. Across workload types (Road Vehicles, Drones), model families (EfficientDet, YOLOX), and model sizes, RedunCut reduces prediction error by $3.5\times$ – $10\times$ vs. Tiered-sampling [46] (Figure 21; §G).

6 Related works

Dynamic model size selection. A number of works have taken advantage of the tradeoff between cost and accuracy across model sizes [99–103]. DMSS is a narrower setup in

which the system navigates this tradeoff per input on live data. This setting is challenging since decision making is more local (lacking access to all video data at a given point in time) and requires finer-grained decisions using rapidly changing information. As discussed in §1 and §2, DMSS has been explored in both video analytics and other applications [46, 48, 49, 53, 54, 104]. We show that these approaches fail to generalize to important workload types and accuracy targets, and we propose RedunCut to fill this gap.

Complementary first-stage data similarity and deduplication methods. Chameleon [46] uses cross-camera similarity to reduce the number of configurations that they sample. Potluck [105] uses a cache-based system to detect duplicated inputs across video sources, and other works [49, 92, 106] explore frame skipping on the same video when they are expected to remain same. Frame dropping is complementary to our method, because (like recent works [6, 7]) we focus on resource allocation to model inference once it is determined that the input cannot be deduplicated or dropped.

“Expert” model training and selection. Recent works [6, 7, 107], present cost-effective methods to boost the accuracy of a small model by fine-tuning it on specific video content at runtime (creating “experts”) using student-teacher learning [108]. To further save cost, RECL [7] proposes a “gating network” to select between previously trained experts. These methods show promise in environments with limited memory and compute. However, when compute and memory are sufficiently available, system designers may prefer to avoid the complexity of training expert models on the fly: Model training requires expertise, and maintaining a large, dynamic pool of models (> 150 experts [7]) is expensive. Further, even after training, expert models may still substantially deviate from the predictions of the teacher model [7, 107]. Instead, in environments with sufficient memory and compute, the teacher model may be run directly.

General model similarity. The use of prediction statistics is part of a line of works that aim to quantify and characterize model differences [109–111]. The methods in these works could be used to improve accuracy prediction at runtime.

7 Conclusion

Dynamic model size selection can significantly reduce LVA cost, but prior methods use manually-crafted rules that oversample and misselect outside their intended workload types and accuracy targets. RedunCut reframes sampling as an explicit cost-benefit decision from historical data, and predicts accuracy using a lightweight performance model. As a model-agnostic shim layer with sequential sampling, RedunCut lowers compute cost by 14–62% for a given accuracy target across diverse workload types, model families, and tasks.

References

- [1] Sokemi Rene Emmanuel Datondji, Yohan Dupuis, Peggy Subirats, and Pascal Vasseur. A survey of vision-based traffic monitoring of road intersections. *IEEE transactions on intelligent transportation systems*, 17(10):2681–2698, 2016.
- [2] Frank Cangialosi, Neil Agarwal, Venkat Arun, Srinivas Narayana, Anand Sarwate, and Ravi Netravali. Privid: practical, Privacy-Preserving video analytics queries. In *19th USENIX Symposium on Networked Systems Design and Implementation (NSDI 22)*, pages 209–228, 2022.
- [3] SecurityInformed editorial team. Video analytics applications in retail - beyond security. <https://www.securityinformed.com/insights/co-2603-ga-co-2214-ga-co-1880-ga.16620.html>.
- [4] Amazon Web Services. Smart store analytics: Creating profitable retail insights. <https://aws.amazon.com/blogs/industries/smart-store-analytics-creating-profitable-retail-insights/>, 2022.
- [5] Voxel51. How computer vision is changing retail. <https://voxel51.com/blog/how-computer-vision-is-changing-retail/>, 2024.
- [6] Romil Bhardwaj, Zhengxu Xia, Ganesh Ananthanarayanan, Junchen Jiang, Yuanchao Shu, Nikolaos Karianakis, Kevin Hsieh, Paramvir Bahl, and Ion Stoica. Ekya: Continuous learning of video analytics models on edge compute servers. In *19th USENIX Symposium on Networked Systems Design and Implementation (NSDI 22)*, pages 119–135, 2022.
- [7] Mehrdad Khani, Ganesh Ananthanarayanan, Kevin Hsieh, Junchen Jiang, Ravi Netravali, Yuanchao Shu, Mohammad Alizadeh, and Victor Bahl. RECL: Responsive Resource-Efficient continuous learning for video analytics. In *20th USENIX Symposium on Networked Systems Design and Implementation (NSDI 23)*, pages 917–932, 2023.
- [8] Ganesh Ananthanarayanan, Paramvir Bahl, Peter Bodík, Krishna Chintalapudi, Matthai Philipose, Lenin Ravindranath, and Sudipta Sinha. Real-time video analytics: The killer app for edge computing. *computer*, 50(10):58–67, 2017.
- [9] Clarion Security Systems. How many CCTV cameras are in london? <https://clarionuk.com/resources/how-many-cctv-cameras-are-in-london/>, 2022.
- [10] Solink Corporation. Video analytics and big data. <https://solink.com/resources/4-comparisons-prove-video-biggest-big-data/>, 2017.
- [11] Monica Davey. As Chicago expands surveillance, a debate surges. <https://www.nytimes.com/2018/05/26/us/chicago-police-surveillance.html>, 2018. *The New York Times*, 26 May 2018.
- [12] Quartz. Absolutely everywhere in Beijing is now covered by police video surveillance. <https://qz.com/518874/absolutely-everywhere-in-beijing-is-now-covered-by-police-video-surveillance>, 2015.
- [13] Tsung-Yi Lin, Piotr Dollár, Ross Girshick, Kaiming He, Bharath Hariharan, and Serge Belongie. Feature pyramid networks for object detection. In *Proceedings of the IEEE conference on computer vision and pattern recognition*, pages 2117–2125, 2017.
- [14] Mingxing Tan, Ruoming Pang, and Quoc V Le. EfficientDet: Scalable and efficient object detection. In *Proceedings of the IEEE/CVF conference on computer vision and pattern recognition*, pages 10781–10790, 2020.
- [15] Zhaowei Cai, Mohammad Saberian, and Nuno Vasconcelos. Learning complexity-aware cascades for deep pedestrian detection. In *Proceedings of the IEEE international conference on computer vision*, pages 3361–3369, 2015.
- [16] Zheng Ge, Songtao Liu, Feng Wang, Zeming Li, and Jian Sun. YOLOX: Exceeding YOLO series in 2021. *arXiv preprint arXiv:2107.08430*, 2021.
- [17] Nicolas Carion, Francisco Massa, Gabriel Synnaeve, Nicolas Usunier, Alexander Kirillov, and Sergey Zagoruyko. End-to-end object detection with transformers. In *European conference on computer vision*, pages 213–229. Springer, 2020.
- [18] Andrew G Howard, Menglong Zhu, Bo Chen, Dmitry Kalenichenko, Weijun Wang, Tobias Weyand, Marco Andreetto, and Hartwig Adam. Mobilenets: Efficient convolutional neural networks for mobile vision applications. *arXiv preprint arXiv:1704.04861*, 2017.
- [19] Xinyu Liu, Houwen Peng, Ningxin Zheng, Yuqing Yang, Han Hu, and Yixuan Yuan. Efficientvit: Memory efficient vision transformer with cascaded group attention. In *Proceedings of the IEEE/CVF conference on computer vision and pattern recognition*, pages 14420–14430, 2023.
- [20] Samvit Jain, Ganesh Ananthanarayanan, Junchen Jiang, Yuanchao Shu, and Joseph Gonzalez. Scaling video analytics systems to large camera deployments. In *Proceedings of the 20th International Workshop on*

- Mobile Computing Systems and Applications*, pages 9–14, 2019.
- [21] Yunzhe Ni, Zhilong Zheng, Xianshang Lin, Fengyu Gao, Xuan Zeng, Yirui Liu, Tao Xu, Hua Wang, Zhi-dong Zhang, Senlang Du, et al. Cellfusion: Multipath vehicle-to-cloud video streaming with network coding in the wild. In *Proceedings of the ACM SIGCOMM 2023 Conference*, pages 668–683, 2023.
- [22] Dongzhu Xu, Anfu Zhou, Guixian Wang, Huanhuan Zhang, Xiangyu Li, Jialiang Pei, and Huadong Ma. Tutti: coupling 5G ran and mobile edge computing for latency-critical video analytics. In *Proceedings of the 28th Annual International Conference on Mobile Computing And Networking*, pages 729–742, 2022.
- [23] 5G technology as the backbone for commercial drone operations. Technical report, GSMA Foundry with Ericsson and TDC NET, 2022. Case study on 5G-enabled UAS with real-time video.
- [24] Mike Wong, Murali Ramanujam, Guha Balakrishnan, and Ravi Netravali. MadEye: Boosting live video analytics accuracy with adaptive camera configurations. In *21st USENIX Symposium on Networked Systems Design and Implementation (NSDI 24)*, pages 549–568, 2024.
- [25] Yiding Wang, Weiyan Wang, Duowen Liu, Xin Jin, Junchen Jiang, and Kai Chen. Enabling edge-cloud video analytics for robotics applications. *IEEE Transactions on Cloud Computing*, 11(2):1500–1513, 2022.
- [26] Kien Nguyen, Clinton Fookes, Sridha Sridharan, Yingli Tian, Feng Liu, Xiaoming Liu, and Arun Ross. The state of aerial surveillance: A survey. *arXiv preprint arXiv:2201.03080*, 2022.
- [27] National Safety Council. Advanced driver assistance systems (adas). <https://injuryfacts.nsc.org/motor-vehicle/occupant-protection/advanced-driver-assistance-systems/data-details/>, 2024.
- [28] Shanhe Yi, Zijiang Hao, Qingyang Zhang, Quan Zhang, Weisong Shi, and Qun Li. Lavea: Latency-aware video analytics on edge computing platform. In *Proceedings of the Second ACM/IEEE Symposium on Edge Computing*, pages 1–13, 2017.
- [29] Qingyang Zhang, Hui Sun, Xiaopei Wu, and Hong Zhong. Edge video analytics for public safety: A review. *Proceedings of the IEEE*, 107(8):1675–1696, 2019.
- [30] Osama ElSahly and Akmal Abdelfatah. A systematic review of traffic incident detection algorithms. *Sustainability*, 14(22):14859, 2022.
- [31] Mingyang Lyu, Yibo Zhao, Chao Huang, and Hailong Huang. Unmanned aerial vehicles for search and rescue: A survey. *Remote Sensing*, 15(13):3266, 2023.
- [32] Julius Pesonen, Anna-Maria Raita-Hakola, Jukka Joutsalainen, Teemu Hakala, Waleed Akhtar, Niko Koivumäki, Lauri Markelin, Juha Suomalainen, Raquel Alves de Oliveira, Ilkka Pölönen, et al. Boreal forest fire: UAV-collected wildfire detection and smoke segmentation dataset. *Scientific Data*, 12(1):1419, 2025.
- [33] Emerging agricultural technologies workgroup report and recommendations for PPDC review. Technical report, U.S. Environmental Protection Agency (EPA), Office of Pesticide Programs.
- [34] Rajib Debnath and Mrinal Kanti Bhowmik. A comprehensive survey on computer vision based concepts, methodologies, analysis and applications for automatic gun/knife detection. *Journal of Visual Communication and Image Representation*, 78:103165, 2021.
- [35] National Institute for Congestion Reduction (NICR). DARTS: Drone-based ai-powered real-time traffic incident detection system. <https://nicr.usf.edu/2024/10/22/darts/>, 2024.
- [36] Francesco Ciccone and Alessandro Ceruti. Real-time search and rescue with drones: A deep learning approach for small-object detection based on YOLO. *Drones*, 9(8):514, 2025.
- [37] Yashar Safyari, Masoud Mahdianpari, and Hodjat Shiri. A review of vision-based pothole detection methods using computer vision and machine learning. *Sensors*, 24(17):5652, 2024.
- [38] Daniel Crankshaw, Xin Wang, Guilio Zhou, Michael J Franklin, Joseph E Gonzalez, and Ion Stoica. Clipper: A Low-Latency online prediction serving system. In *14th USENIX Symposium on Networked Systems Design and Implementation (NSDI 17)*, pages 613–627, 2017.
- [39] Haichen Shen, Lequn Chen, Yuchen Jin, Liangyu Zhao, Bingyu Kong, Matthai Philipose, Arvind Krishnamurthy, and Ravi Sundaram. Nexus: A GPU cluster engine for accelerating dnn-based video analysis. In *Proceedings of the 27th ACM Symposium on Operating Systems Principles*, pages 322–337, 2019.
- [40] Lianmin Zheng, Zhuohan Li, Hao Zhang, Yonghao Zhuang, Zhifeng Chen, Yanping Huang, Yida Wang, Yuanzhong Xu, Danyang Zhuo, Eric P Xing, et al. Alpa: Automating inter-and Intra-Operator parallelism for distributed deep learning. In *16th USENIX Symposium on Operating Systems Design and Implementation (OSDI 22)*, pages 559–578, 2022.

- [41] Francisco Romero, Qian Li, Neeraja J Yadwadkar, and Christos Kozyrakis. INFaaS: Automated model-less inference serving. In *2021 USENIX Annual Technical Conference (USENIX ATC 21)*, pages 397–411, 2021.
- [42] Anand Padmanabha Iyer, Mingyu Guan, Yinwei Dai, Rui Pan, Swapnil Gandhi, and Ravi Netravali. Improving DNN inference throughput using practical, per-input compute adaptation. In *Proceedings of the ACM SIGOPS 30th Symposium on Operating Systems Principles*, pages 624–639, 2024.
- [43] Yinwei Dai, Rui Pan, Anand Iyer, Kai Li, and Ravi Netravali. Apparate: Rethinking early exits to tame latency-throughput tensions in ml serving. In *Proceedings of the ACM SIGOPS 30th Symposium on Operating Systems Principles*, pages 607–623, 2024.
- [44] Noam Shazeer, Azalia Mirhoseini, Krzysztof Maziarz, Andy Davis, Quoc Le, Geoffrey Hinton, and Jeff Dean. Outrageously large neural networks: The sparsely-gated mixture-of-experts layer. *arXiv preprint arXiv:1701.06538*, 2017.
- [45] Jiamin Li, Yimin Jiang, Yibo Zhu, Cong Wang, and Hong Xu. Accelerating distributed MoE training and inference with lina. In *2023 USENIX Annual Technical Conference (USENIX ATC 23)*, pages 945–959, 2023.
- [46] Junchen Jiang, Ganesh Ananthanarayanan, Peter Bodik, Siddhartha Sen, and Ion Stoica. Chameleon: scalable adaptation of video analytics. In *Proceedings of the 2018 conference of the ACM special interest group on data communication*, pages 253–266, 2018.
- [47] Xin Wang, Yujia Luo, Daniel Crankshaw, Alexey Tumanov, Fisher Yu, and Joseph E Gonzalez. Idk cascades: Fast deep learning by learning not to overthink. *arXiv preprint arXiv:1706.00885*, 2017.
- [48] Yiding Wang, Kai Chen, Haisheng Tan, and Kun Guo. Tabi: An efficient multi-level inference system for large language models. In *Proceedings of the Eighteenth European Conference on Computer Systems*, pages 233–248, 2023.
- [49] Daniel Kang, John Emmons, Firas Abuzaid, Peter Bailis, and Matei Zaharia. Noscope: Optimizing neural network queries over video at scale. *Proceedings of the VLDB Endowment*, 10(11), 2017.
- [50] Haoyu Zhang, Ganesh Ananthanarayanan, Peter Bodik, Matthai Philipose, Paramvir Bahl, and Michael J Freedman. Live video analytics at scale with approximation and Delay-Tolerance. In *14th USENIX Symposium on Networked Systems Design and Implementation (NSDI 17)*, pages 377–392, 2017.
- [51] Kuntai Du, Ahsan Pervaiz, Xin Yuan, Aakanksha Chowdhery, Qizheng Zhang, Henry Hoffmann, and Junchen Jiang. Server-driven video streaming for deep learning inference. In *Proceedings of the Annual conference of the ACM Special Interest Group on Data Communication on the applications, technologies, architectures, and protocols for computer communication*, pages 557–570, 2020.
- [52] Luyang Liu, Hongyu Li, and Marco Gruteser. Edge assisted real-time object detection for mobile augmented reality. In *The 25th annual international conference on mobile computing and networking*, pages 1–16, 2019.
- [53] Shiqi Jiang, Zhiqi Lin, Yuanchun Li, Yuanchao Shu, and Yunxin Liu. Flexible high-resolution object detection on edge devices with tunable latency. In *Proceedings of the 27th Annual International Conference on Mobile Computing and Networking*, pages 559–572, 2021.
- [54] Michael R Anderson, Michael Cafarella, German Ros, and Thomas F Wenisch. Physical representation-based predicate optimization for a visual analytics database. In *2019 IEEE 35th International Conference on Data Engineering (ICDE)*, pages 1466–1477. IEEE, 2019.
- [55] Christina Delimitrou and Christos Kozyrakis. Paragon: Qos-aware scheduling for heterogeneous datacenters. *ACM SIGPLAN Notices*, 48(4):77–88, 2013.
- [56] Christina Delimitrou and Christos Kozyrakis. Quasar: Resource-efficient and qos-aware cluster management. *ACM Sigplan Notices*, 49(4):127–144, 2014.
- [57] Romil Bhardwaj, Kirthevasan Kandasamy, Asim Biswal, Wenshuo Guo, Benjamin Hindman, Joseph Gonzalez, Michael Jordan, and Ion Stoica. Cilantro: Performance-Aware resource allocation for general objectives via online feedback. In *17th USENIX Symposium on Operating Systems Design and Implementation (OSDI 23)*, pages 623–643, 2023.
- [58] Zhuofan Zong, Guanglu Song, and Yu Liu. Detsr with collaborative hybrid assignments training. In *Proceedings of the IEEE/CVF international conference on computer vision*, pages 6748–6758, 2023.
- [59] Xuechen Zhang, Samet Oymak, and Jiasi Chen. Post-hoc models for performance estimation of machine learning inference. *arXiv preprint arXiv:2110.02459*, 2021.
- [60] Zheng Yang, Xu Wang, Jiahang Wu, Yi Zhao, Qiang Ma, Xin Miao, Li Zhang, and Zimu Zhou. Edgeduet: Tiling small object detection for edge assisted autonomous mobile vision. *IEEE/ACM Transactions on Networking*, 31(4):1765–1778, 2022.

- [61] Neil Agarwal and Ravi Netravali. Boggart: Towards General-Purpose acceleration of retrospective video analytics. In *20th USENIX Symposium on Networked Systems Design and Implementation (NSDI 23)*, pages 933–951, 2023.
- [62] Lexin Zhou, Pablo A Moreno-Casares, Fernando Martínez-Plumed, John Burden, Ryan Burnell, Lucy Cheke, Cèsar Ferri, Alexandru Marcoci, Behzad Mehrbakhsh, Yael Moros-Daval, et al. Predictable artificial intelligence. *arXiv preprint arXiv:2310.06167*, 2023.
- [63] Mahdie Karbasi and Dorothea Kolossa. Asr-based speech intelligibility prediction: A review. *Hearing Research*, 426:108606, 2022.
- [64] Lorenzo Pacchiardi, Konstantinos Voudouris, Ben Slater, Fernando Martínez-Plumed, José Hernández-Orallo, Lexin Zhou, and Wout Schellaert. Predictaboard: Benchmarking LLM score predictability. *arXiv preprint arXiv:2502.14445*, 2025.
- [65] Mingyu Liang, Hiwot Tadese Kassa, Wenyin Fu, Brian Coutinho, Louis Feng, and Christina Delimitrou. Lumos: Efficient performance modeling and estimation for large-scale LLM training. *arXiv preprint arXiv:2504.09307*, 2025.
- [66] Pei Sun, Henrik Kretschmar, Xerxes Dotiwalla, Aurelien Chouard, Vijaysai Patnaik, Paul Tsui, James Guo, Yin Zhou, Yuning Chai, Benjamin Caine, et al. Scalability in perception for autonomous driving: Waymo open dataset. In *Proceedings of the IEEE/CVF conference on computer vision and pattern recognition*, pages 2446–2454, 2020.
- [67] Yaniv Ovadia, Emily Fertig, Jie Ren, Zachary Nado, David Sculley, Sebastian Nowozin, Joshua Dillon, Balaji Lakshminarayanan, and Jasper Snoek. Can you trust your model’s uncertainty? evaluating predictive uncertainty under dataset shift. *Advances in neural information processing systems*, 32, 2019.
- [68] Emmanouil Antonios Platanios, Avinava Dubey, and Tom Mitchell. Estimating accuracy from unlabeled data: A bayesian approach. In *International Conference on Machine Learning*, pages 1416–1425. PMLR, 2016.
- [69] Chuan Guo, Geoff Pleiss, Yu Sun, and Kilian Q Weinberger. On calibration of modern neural networks. In *International conference on machine learning*, pages 1321–1330. PMLR, 2017.
- [70] Omid Alipourfard, Hongqiang Harry Liu, Jianshu Chen, Shivaram Venkataraman, Minlan Yu, and Ming Zhang. CherryPick: Adaptively unearthing the best cloud configurations for big data analytics. In *14th USENIX Symposium on Networked Systems Design and Implementation (NSDI 17)*, pages 469–482, 2017.
- [71] Shivaram Venkataraman, Zongheng Yang, Michael Franklin, Benjamin Recht, and Ion Stoica. Ernest: Efficient performance prediction for Large-Scale advanced analytics. In *13th USENIX symposium on networked systems design and implementation (NSDI 16)*, pages 363–378, 2016.
- [72] Yanqi Zhang, Weizhe Hua, Zhuangzhuang Zhou, G Edward Suh, and Christina Delimitrou. Sinan: MI-based and qos-aware resource management for cloud microservices. In *Proceedings of the 26th ACM international conference on architectural support for programming languages and operating systems*, pages 167–181, 2021.
- [73] Andrew D Ferguson, Peter Bodik, Srikanth Kandula, Eric Boutin, and Rodrigo Fonseca. Jockey: guaranteed job latency in data parallel clusters. In *Proceedings of the 7th ACM european conference on Computer Systems*, pages 99–112, 2012.
- [74] Mingzhe Hao, Levent Toksoz, Nanqinqin Li, Edward Edberg Halim, Henry Hoffmann, and Haryadi S Gunawi. LinnOS: Predictability on unpredictable flash storage with a light neural network. In *14th USENIX Symposium on Operating Systems Design and Implementation (OSDI 20)*, pages 173–190, 2020.
- [75] Xukan Ran, Haolianz Chen, Xiaodan Zhu, Zhenming Liu, and Jiasi Chen. Deepdecision: A mobile deep learning framework for edge video analytics. In *IEEE INFOCOM 2018-IEEE conference on computer communications*, pages 1421–1429. IEEE, 2018.
- [76] Yiwen Zhang, Xumiao Zhang, Ganesh Ananthanarayanan, Anand Iyer, Yuanchao Shu, Victor Bahl, Z Morley Mao, and Mosharaf Chowdhury. Vulcan: Automatic query planning for live ML analytics. In *21st USENIX Symposium on Networked Systems Design and Implementation (NSDI 24)*, pages 1385–1402, 2024.
- [77] Larry Wasserman. *All of statistics: a concise course in statistical inference*. Springer Science & Business Media, 2013.
- [78] Christopher D Manning. *Introduction to information retrieval*. Syngress Publishing,, 2008.
- [79] Alan Agresti and Maria Kateri. Categorical data analysis. In *International encyclopedia of statistical science*, page 22. Springer, 2025.

- [80] Trevor Hastie. The elements of statistical learning: data mining, inference, and prediction, 2009.
- [81] Han Jiawei and Kamber Micheline. *Data mining: concepts and techniques*. Morgan kaufmann, 2006.
- [82] State of practice for automated incident detection - final report. Technical report, ENTERPRISE Transportation Pooled Fund Program, 2022.
- [83] Philipp Moritz, Robert Nishihara, Stephanie Wang, Alexey Tumanov, Richard Liaw, Eric Liang, Melih Elilbol, Zongheng Yang, William Paul, Michael I Jordan, et al. Ray: A distributed framework for emerging AI applications. In *13th USENIX symposium on operating systems design and implementation (OSDI 18)*, pages 561–577, 2018.
- [84] Ray serve. <https://docs.ray.io/en/latest/serve/index.html>.
- [85] Pengfei Zhu, Longyin Wen, Xiao Bian, Haibin Ling, and Qinghua Hu. Vision meets drones: A challenge. *arXiv preprint arXiv:1804.07437*, 2018.
- [86] Kellie Corona, Katie Osterdahl, Roderic Collins, and Anthony Hoogs. MEVA: A large-scale multiview, multimodal video dataset for activity detection. In *Proceedings of the IEEE/CVF winter conference on applications of computer vision*, pages 1060–1068, 2021.
- [87] Alex Bewley, Zongyuan Ge, Lionel Ott, Fabio Ramos, and Ben Upcroft. Simple online and realtime tracking. In *2016 IEEE international conference on image processing (ICIP)*, pages 3464–3468. IEEE, 2016.
- [88] Martín Abadi, Paul Barham, Jianmin Chen, Zhifeng Chen, Andy Davis, Jeffrey Dean, Matthieu Devin, Sanjay Ghemawat, Geoffrey Irving, Michael Isard, et al. TensorFlow: a system for Large-Scale machine learning. In *12th USENIX symposium on operating systems design and implementation (OSDI 16)*, pages 265–283, 2016.
- [89] Tsung-Yi Lin, Michael Maire, Serge Belongie, James Hays, Pietro Perona, Deva Ramanan, Piotr Dollár, and C Lawrence Zitnick. Microsoft COCO: Common objects in context. In *Computer Vision—ECCV 2014: 13th European Conference, Zurich, Switzerland, September 6-12, 2014, Proceedings, Part V 13*, pages 740–755. Springer, 2014.
- [90] Kaiming He, Georgia Gkioxari, Piotr Dollár, and Ross Girshick. Mask R-CNN. In *Proceedings of the IEEE international conference on computer vision*, pages 2961–2969, 2017.
- [91] Anton Milan, Laura Leal-Taixé, Ian Reid, Stefan Roth, and Konrad Schindler. MOT16: A benchmark for multi-object tracking. *arXiv preprint arXiv:1603.00831*, 2016.
- [92] Yuanqi Li, Arthi Padmanabhan, Pengzhan Zhao, Yufei Wang, Guoqing Harry Xu, and Ravi Netravali. Reducto: On-camera filtering for resource-efficient real-time video analytics. In *Proceedings of the Annual conference of the ACM Special Interest Group on Data Communication on the applications, technologies, architectures, and protocols for computer communication*, pages 359–376, 2020.
- [93] Jeffrey Ouyang-Zhang, Jang Hyun Cho, Xingyi Zhou, and Philipp Krähenbühl. NMS strikes back. *arXiv preprint arXiv:2212.06137*, 2022.
- [94] Bin Yan, Yi Jiang, Peize Sun, Dong Wang, Zehuan Yuan, Ping Luo, and Huchuan Lu. Towards grand unification of object tracking. In *European Conference on Computer Vision*, pages 733–751. Springer, 2022.
- [95] Kaiming He, Xiangyu Zhang, Shaoqing Ren, and Jian Sun. Deep residual learning for image recognition. In *Proceedings of the IEEE conference on computer vision and pattern recognition*, pages 770–778, 2016.
- [96] Gal Kaplun, Nikhil Ghosh, Saurabh Garg, Boaz Barak, and Preetum Nakkiran. Deconstructing distributions: A pointwise framework of learning. *arXiv preprint arXiv:2202.09931*, 2022.
- [97] Mark Weber, Jun Xie, Maxwell Collins, Yukun Zhu, Paul Voigtlaender, Hartwig Adam, Bradley Green, Andreas Geiger, Bastian Leibe, Daniel Cremers, et al. Step: Segmenting and tracking every pixel. *arXiv preprint arXiv:2102.11859*, 2021.
- [98] Sijie Dong, Qitong Wang, Soror Sahri, Themis Palpanas, and Divesh Srivastava. Efficiently mitigating the impact of data drift on machine learning pipelines. *Proceedings of the VLDB Endowment*, 17(11):3072–3081, 2024.
- [99] Wei Wang, Sheng Wang, Jinyang Gao, Meihui Zhang, Gang Chen, Teck Khim Ng, and Beng Chin Ooi. Rafiki: Machine learning as an analytics service system. *arXiv preprint arXiv:1804.06087*, 2018.
- [100] Jiashen Cao, Karan Sarkar, Ramyad Hadidi, Joy Arulraj, and Hyesoon Kim. FiGO: Fine-grained query optimization in video analytics. In *Proceedings of the 2022 International conference on management of data*, pages 559–572, 2022.

- [101] Peizhen Guo, Bo Hu, and Wenjun Hu. Sommelier: Curating dnn models for the masses. In *Proceedings of the 2022 International Conference on Management of Data*, pages 1876–1890, 2022.
- [102] Jashwant Raj Gunasekaran, Cyan Subhra Mishra, Prashanth Thinakaran, Bikash Sharma, Mahmut Taylan Kandemir, and Chita R Das. Cocktail: A multidimensional optimization for model serving in cloud. In *19th USENIX Symposium on Networked Systems Design and Implementation (NSDI 22)*, pages 1041–1057, 2022.
- [103] Sohaib Ahmad, Hui Guan, Brian D Friedman, Thomas Williams, Ramesh K Sitaraman, and Thomas Woo. Proteus: A high-throughput inference-serving system with accuracy scaling. In *Proceedings of the 29th ACM International Conference on Architectural Support for Programming Languages and Operating Systems, Volume 1*, pages 318–334, 2024.
- [104] Kevin Hsieh, Ganesh Ananthanarayanan, Peter Bodik, Shivaram Venkataraman, Paramvir Bahl, Matthai Philipose, Phillip B Gibbons, and Onur Mutlu. Focus: Querying large video datasets with low latency and low cost. In *13th USENIX Symposium on Operating Systems Design and Implementation (OSDI 18)*, pages 269–286, 2018.
- [105] Peizhen Guo and Wenjun Hu. Potluck: Cross-application approximate deduplication for computation-intensive mobile applications. In *Proceedings of the Twenty-Third International Conference on Architectural Support for Programming Languages and Operating Systems*, pages 271–284, 2018.
- [106] Christopher Canel, Thomas Kim, Giulio Zhou, Conglong Li, Hyeontaek Lim, David G Andersen, Michael Kaminsky, and Subramanya Dulloor. Scaling video analytics on constrained edge nodes. *Proceedings of Machine Learning and Systems*, 1:406–417, 2019.
- [107] Mehrdad Khani, Pouya Hamadani, Arash Nasr-Esfahany, and Mohammad Alizadeh. Real-time video inference on edge devices via adaptive model streaming. In *Proceedings of the IEEE/CVF International Conference on Computer Vision*, pages 4572–4582, 2021.
- [108] Geoffrey Hinton, Oriol Vinyals, and Jeff Dean. Distilling the knowledge in a neural network. *arXiv preprint arXiv:1503.02531*, 2015.
- [109] Hengrui Jia, Hongyu Chen, Jonas Guan, Ali Shahin Shamsabadi, and Nicolas Papernot. A zest of lime: Towards architecture-independent model distances. In *International Conference on Learning Representations*, 2021.
- [110] Harshay Shah, Sung Min Park, Andrew Ilyas, and Aleksander Madry. Modeldiff: A framework for comparing learning algorithms. In *International Conference on Machine Learning*, pages 30646–30688. PMLR, 2023.
- [111] Max Klabunde, Tobias Schumacher, Markus Strohmaier, and Florian Lemmerich. Similarity of neural network models: A survey of functional and representational measures. *ACM Computing Surveys*, 57(9):1–52, 2025.

Supplementary Material: Table of contents

- Control parameter search details (§A)
- Gating network adaptation limitation (§B)
- Multi-object tracker cascade design (§C)
- MEVA and VisDrone main results (§D)
- Spearman correlation between prediction statistics and accuracy (§E)
- Optimal number of models to sample in different settings (§F)
- Accuracy prediction error (§G)
- Correlations between prediction statistics (§H)
- Selector ablation (§I)

A Control parameter search details

Tiered-sampling. The following knobs are left as control parameters which we search and find separately as described in §5.1: profiling window length, segment length, subsegment profiling duration, the configuration subset size k , and the size of the reference model used as ground truth when sampling the top- k .

B Gating network adaptation limitation

Why doesn't the gating network reach the top-right of the tradeoff space? This happens because of the way that the gating neural network in RECL [7] is adapted to model size selection in our setting. The adaptation trains the gating network to select the model size that optimizes the cost-accuracy objective used in RedunCut. The downside of this approach is that when the objective is set to prioritize maximizing accuracy (with no limit on cost), 49% of the model size labels (in the Waymo dataset) are not the largest model size. This takes place in scenarios in which a small model has an accuracy equal to or (occasionally) greater than the accuracy of the large model [96]. As a result, the gating network that is adapted for model size selection is never trained to select the largest model for all video segments.

C Multi-object tracker cascade design

To the best of our knowledge, there are no known works that have adapted a model cascade for multi-object tracking. Therefore, we develop the following confidence-score based early-exit rule: the smaller model is run on the frame, and the resulting object predictions with a confidence score in the range $[l, h)$ are recorded by the cascade. Then, their average confidence score m is computed and compared against a confidence threshold c . When $m < c$, the larger model is run next and its predictions are chosen for the frame. Otherwise, the larger model is not run and the predictions of the smaller model are chosen for the frame. l , h , and c are left as control parameters that are searched as described in §5.1.

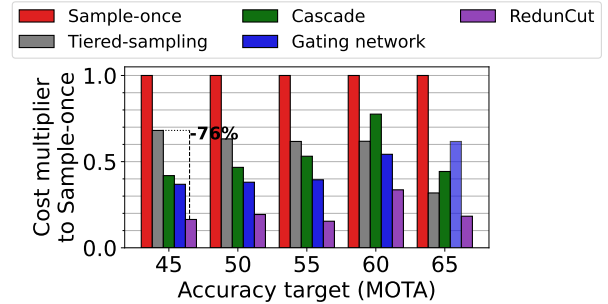


Figure 16: The normalized compute cost of RedunCut and other video analytics methods in surveillance camera videos. Each method (color) is evaluated on a range of accuracy targets (x-axis). The resulting compute cost is normalized by dividing it by the compute cost of the sample-once method (y-axis). The single translucent blue bar is described in §5.2.

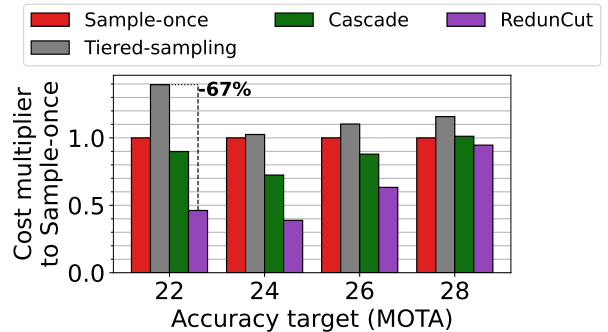


Figure 17: The normalized compute cost of RedunCut and other video analytics methods in drone camera videos. Each method (color) is evaluated on a range of accuracy targets (x-axis). The resulting compute cost is normalized by dividing it by the compute cost of the sample-once method (y-axis).

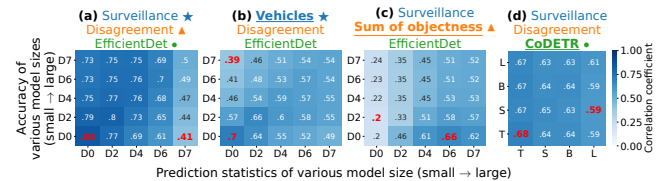


Figure 18: Spearman correlation between the prediction statistics and the accuracy.

D MEVA and VisDrone main results

Figure 16 and Figure 17 show the main results from Figure 8 in barplot form.

E Spearman correlation between prediction statistics and accuracy

See Figure 18.

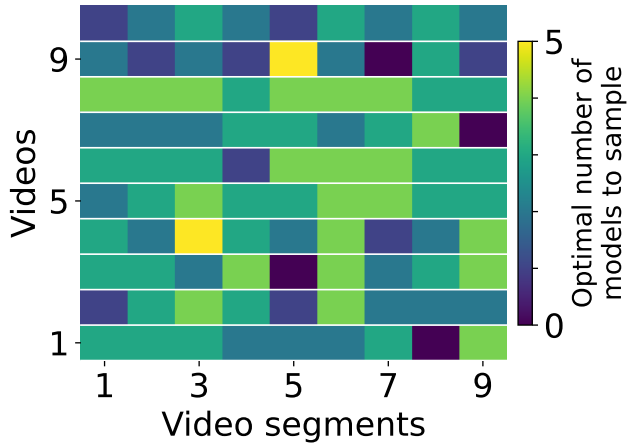


Figure 19: The optimal number of models to sample in different segments of videos. The optimal number of models to sample (color) across different video segments (x-axis) of different videos (y-axis).

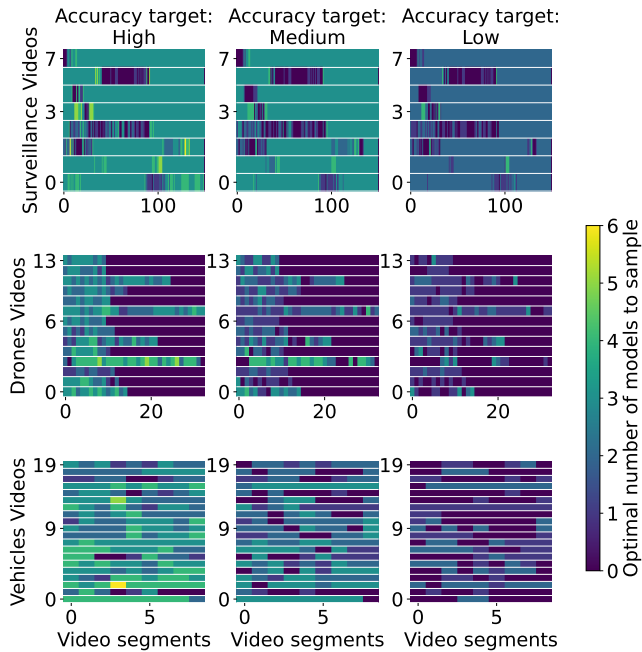


Figure 20: The optimal number of models to sample in different accuracy targets and workload types.

F Optimal number of models to sample in different settings

See Figure 19 and Figure 20.

G Accuracy prediction error

See Figure 21.

H Correlations between prediction statistics

See Figure 22.

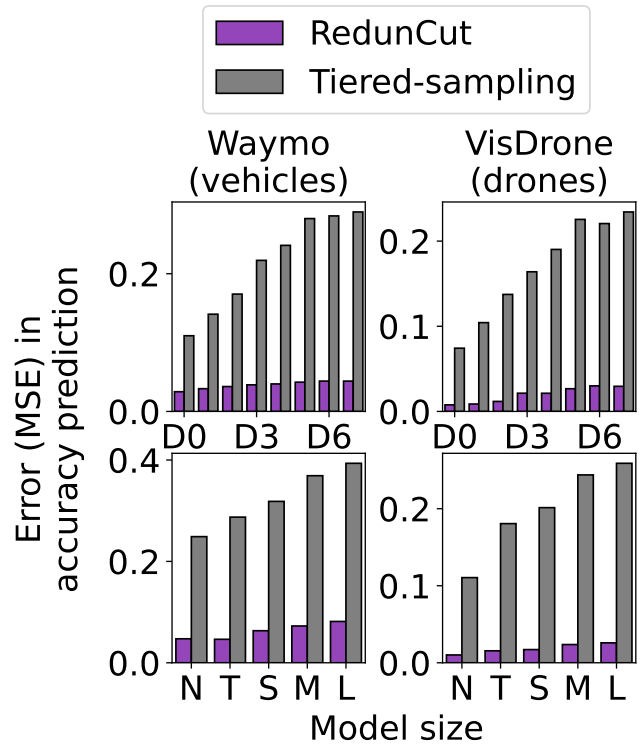


Figure 21: The error of different accuracy prediction methods. The error of accuracy prediction (Mean-squared error, y-axis) of different methods (color) across different datasets (left/right), model families (top/bottom), and different model sizes (x-axis). RedunCut’s error is $3.4\text{-}10\times$ lower than the error that Tiered-sampling [46] achieves using the model disagreement score [6, 7, 46, 50].

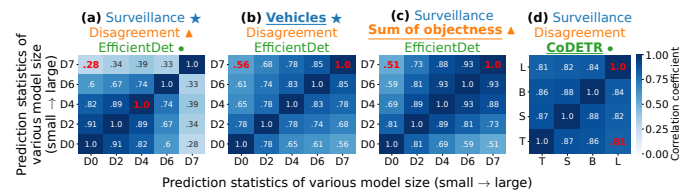


Figure 22: Correlation among prediction statistics. The correlation (Pearson) between the prediction statistics of different model sizes across workload types, prediction statistics types, and model families. See the caption of Figure 6 for information about the headings and comparison between (a) - (d).

I Selector ablation

See Figure 23.

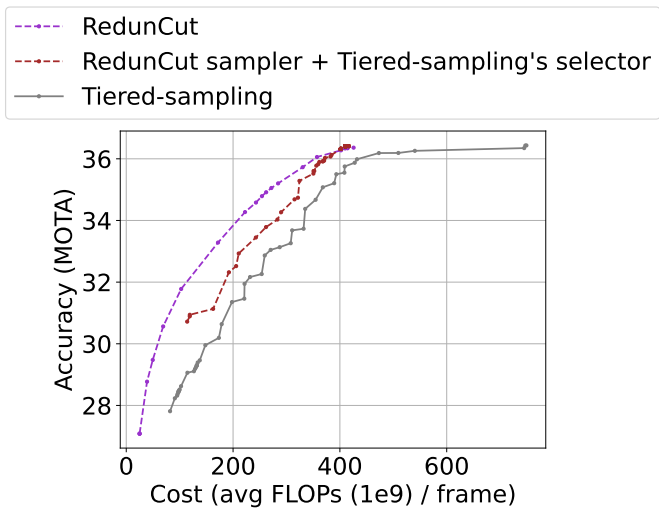


Figure 23: An ablation of RedunCut's selection mechanism.